# Figures of merit for 2D surface plasmon waveguides and application to metal stripes

**Robin Buckley[1] and Pierre Berini[1,2]**

[1]*School of Information Technology and Engineering (SITE), University of Ottawa, 161 Louis Pasteur Ottawa ON, K1N 6N5, Canada*
[2]*Spectalis Corporation, PO Box 72029, Kanata North RPO, Ottawa ON, K2K 2P4, Canada*
*pierreberini@spectalis.com, berini@site.uottawa.ca*

**Abstract:** Three figures of merit, useful as quality measures for 2D surface plasmon waveguides, are discussed and applied to help trade-off mode confinement against attenuation for the symmetric mode propagating along metal stripes. Different stripe geometries are considered, and Au, Ag and Al are compared as the stripe metal over the wavelength range from 200 to 2000 nm. Depending on which figure of merit is used, and on how mode confinement is measured, different preferred designs emerge. For instance, given a mode area, narrow thick stripes are better than wide thin ones, but given a distance from the light line, the opposite is true. Each of the metals analyzed show wavelength regions where their performance is best. The figures of merit are generally applicable and should be useful to help compare, assess and optimize designs in other 2D surface plasmon waveguides or in other absorbing waveguides.



**OCIS codes:** (240.6680) Surface Plasmons; (130.2790) Guided waves.

## References and Links

1. M. Bass *et al.*(Editors), "Properties of Metals," in *Handbook of Optics – Vol II*, (McGraw-Hill, 2000).
2. H. Raether, *Surface Plasmons on Smooth and Rough Surfaces and on Gratings* (Springer, Berlin, 1988).
3. K. Welford, "Surface plasmon-polaritons and their uses," Opt. Quantum Electron. **23**, 1-27 (1991).
4. W. L. Barnes, "Surface plasmon-polaritons length scales: a route to sub-wavelength optics," J. Opt. A: Pure Appl. Opt. **8**, S87-S93 (2006).
5. W. L. Barnes, A. Dereux and T. W. Ebbesen, "Surface plasmon subwavelength optics," Nat. **424**, 824-830 (2003).
6. S. A. Maier and H. A. Atwater, "Plasmonics: Localization and guiding of electromagnetic energy in metal/dielectric structures," J. Appl. Phys. **98**, 011101 (2005).
7. D. Sarid, "Long-range surface-plasma waves on very thin metal films," Phys. Rev. Lett. **47**, 1927-1930 (1981).
8. J. J. Burke, G. I. Stegeman, and T. Tamir, "Surface-polariton-like waves guided by thin, lossy metal films," Phys. Rev. B **33**, 5186-5201 (1986).
9. P. Berini, "Plasmon-polariton modes guided by a metal film of a finite width," Opt. Lett. **24**, 1011-1013 (1999).
10. P. Berini, "Plasmon polariton waves guided by thin lossy metal films of finite width: bound modes of symmetric structures," Phys. Rev. B **61**, 10484-10503 (2000).
11. A. Degiron and D. Smith, "Numerical simulations of long-range plasmons", Opt. Express **14,** 1611-1625 (2006).
12. R. Charbonneau, N. Lahoud, G. Mattiussi and P. Berini, "Demonstration of integrated optics elements based on long-ranging surface plasmon polaritons," Opt. Express **13**, 977-984 (2005).
13. R. Charbonneau, C. Scales, I. Breukelaar, S. Fafard, N. Lahoud, G. Mattiussi, and P. Berini, "Passive integrated optics elements based on long-range surface plasmon polaritons," J. Lightwave Technol. **24**, 447-494 (2006).
14. S. Jetté-Charbonneau, R. Charbonneau, N. Lahoud, G. Mattiussi, and P. Berini, "Demonstration of Bragg gratings based on long-ranging surface plasmon polariton waveguides," Opt. Express **13**, 4674-4682 (2005).
15. A. Boltasseva, T. Nikolajsen, K. Leosson, K. Kjaer, M. S. Larsen and S. I. Bozhevolnyi, "Integrated Optical Components Utilizing Long-Range Surface Plasmon Polaritons," J. Lightwave Technol. **23**, 413-422 (2005).
16. A. Boltasseva, S. I. Bozhevolnyi, T. Nikolajsen, and K. Leosson, "Compact Bragg Gratings for Long-Range Surface Plasmon Polaritons," J. Lightwave Technol. **24**, 912-918 (2006).
17. B. Lamprecht, J. R. Krenn, G. Schider, H. Ditlbacher, M. Salerno, N. Felidj, A. Leitner and F.R. Aussenegg, "Surface plasmon propagation in microscale metal stripes," Appl. Phys. Lett. **79,** 51-53 (2001).

#84184 - $15.00 USD Received 15 Jun 2007; revised 3 Sep 2007; accepted 3 Sep 2007; published 10 Sep 2007

18. J.-C. Weeber, J. R. Krenn, A. Dereux, B. Lamprecht, Y. Lacroute, and J.-P. Goudonnet, "Near-field observation of surface plasmon polariton propagation on thin metal stripes," Phys. Rev. B **64**, 045411 (2001).
19. J.-C. Weeber, A. Dereux, C. Girard, J. R. Krenn and J.-P. Goudonnet, "Plasmon polaritons of metallic nanowires for controlling submicron propagation of light," Phys. Rev. B **60**, 9061-9068 (1999).
20. R. Zia, M. D. Selker, P. B. Catrysse and M. L. Brongersma, "Geometries and materials for subwavelength surface plasmon modes," J. Opt. Soc. Am. A **21**, 2442-2446 (2004).
21. K. R. Welford and J. R. Sambles, "Coupled Surface Plasmons in a Symmetric System", J. Mod. Opt. **35**, 1467-1483 (1988).
22. J. A. Dionne, L. A. Sweatlock, H. A. Atwater and A. Polman, "Plasmon slot waveguides: Towards chip-scale propagation with subwavelength-scale localization" Phys. Rev. B **73**, 035407 (2006).
23. I. V. Novikov and A. A. Maradudin, "Channel Polaritons," Phys. Rev. B **66**, 035403 (2002).
24. D. F. P. Pile and D. K. Gramotnev, "Channel plasmon-polariton in a triangular groove on a metal surface," Opt. Lett. **29**, 1069-1071 (2004) http://www.opticsinfobase.org/abstract.cfm?URI=ol-29-10-1069
25. S. I. Bozhevolnyi, V. S. Volkov, E. Devaux, and T. W. Ebbesen, "Channel plasmon-polariton guiding by subwavelength metal grooves," Phys. Rev. Lett. **95**, 046802 (2005).
26. P. Berini, "Figures of merit for surface plasmon waveguides," Opt. Express **14**, 13030-13042 (2006).
27. J. Guo and R. Adato, "Extended long range plasmon waves in finite thickness metal film and layered dielectric materials," Opt. Express **14**, 12409-12418 (2006).
28. A. Degiron, C. Dellagiacoma, J. G. McIlhargey, G. Shvets, O. J. F. Martin, and D. R. Smith, "Simulations of hybrid long-range plasmon modes with application to 90° bends," Opt. Lett. **32**, 2354-2356 (2007) http://www.opticsinfobase.org/abstract.cfm?URI=ol-32-16-2354
29. P. Berini, R. Charbonneau, and N. Lahoud, "Long-Range Surface Plasmons on Ultrathin Membranes," Nano Lett. **7**, 1376-1380 (2007).
30. C. Chen, P. Berini, D. Feng, S. Tanev, and V. Tzolov, "Efficient and accurate numerical analysis of multilayer planar optical waveguides in lossy anisotropic media," Opt. Express **7**, 260-272 (2000).
31. I. Breukelaar, R. Charbonneau, and P. Berini, "Long-range surface plasmon-polariton mode cutoff and radiation in embedded strip waveguides," J. Appl. Phys. **100**, 043104 (2006).
32. E. D. Palik (Editor), *Handbook of Optical Constants of Solids*, (Academic Press, Orlando, Florida, 1985).
33. P. Berini, R. Charbonneau, N. Lahoud, and G. Mattiussi, "Characterization of long-range surface-plasmon-polariton waveguides," J. Appl. Phys. **98**, 043109 (2005).

## 1. Introduction

The optical properties of metals have been studied and are known to exhibit a negative real part of permittivity at optical frequencies [1]. This property allows the metal-dielectric interface to support a surface plasmon-polariton (SPP) mode which is bound to the interface through the coupling of electromagnetic waves to oscillations in conduction electrons in the metal. The SPP has been studied extensively, and has been reviewed by Raether [2], Welford [3], Barnes [4,5], Maier and Atwater [6] among others. The high loss of the single interface SPP makes it, in general, incapable of long range transmission.

A thin metal slab bounded by dielectric supports bound supermodes, labeled $s_b$ and $a_b$ [7,8]. As the thickness of the slab approaches zero the attenuation of the $s_b$ mode, or long-range SPP (LRSPP), decreases and the mode becomes less confined eventually evolving into the TEM wave of the background dielectric. When the width of the thin metal slab is made finite, defining a stripe, and the metal stripe is embedded in a homogeneous background dielectric, then a more complicated set of modes emerge [9,10,11] since the stripe provides 2D confinement in the plane transverse to the direction of propagation. For a sufficiently thin or narrow metal stripe, the $ss_b^0$ mode becomes long-range (it is the LRSPP). Numerous LRSPP passive devices such as Mach-Zehnder interferometers, Y-junctions, directional couplers [12,13] and Bragg gratings [14], excited by butt-coupling with an optical fiber, have been experimentally tested and shown to closely agree with theory. Similar devices were also reported in [15,16]. The metal stripe exposed to air has also been studied [17-19].

The metal slab and stripe exhibit a trade-off with regards to the confinement and attenuation of the LRSPP supported therein: The confinement and attenuation of the LRSPP rise and fall together [10,20]. This trade-off also applies to other SPP waveguides such as the single-interface, the metal cladded dielectric slab [21,22] and the channel waveguide [23-25], for example. The attenuation-confinement trade-off in surface plasmon waveguides was recently discussed in [26], where three FoMs (figures of merit), denoted $M_1^{1D}$, $M_2$ and $M_3$,

#84184 - $15.00 USD Received 15 Jun 2007; revised 3 Sep 2007; accepted 3 Sep 2007; published 10 Sep 2007

were proposed to assist with trade-off analyses. The FoMs were then used to study three 1D waveguides: the single-interface, the metal slab and the metal cladded dielectric slab [26].

In this paper, we extend the $M_1^{1D}$ FoM proposed in [26] to 2D waveguides, defining the new variant $M_1^{2D}$ (Section 2), and we use the three FoMs ($M_1^{2D}$, $M_2$ and $M_3$) to study the LRSPP in the metal stripe as a function of geometry (Section 3) and metal choice (Au, Ag and Al - Section 4). Section 5 gives a brief summary and conclusions.

## 2. Figures of merit for 2D waveguides

An $\exp(j\omega t)$ time dependence is assumed with mode propagation occurring along the +z axis with an $\exp(-\gamma_z z)$ dependence, where $\omega$ is the angular frequency and $\gamma_z = \alpha_z + j\beta_z$ is the complex propagation constant with $\alpha_z$ and $\beta_z$ the attenuation and phase constants, respectively. The complex effective index $N_{eff}$ is given by $N_{eff} = \gamma_z/\beta_0 = k_{eff} + jn_{eff}$ where $\beta_0 = 2\pi/\lambda_0$ is the free-space phase constant and $\lambda_0$ is the free-space operating wavelength.

### *2.1 Figures of merit: $M_1^{1D}$, $M_2$ and $M_3$*

Three FoMs were defined in [26] to provide objective measures of comparison for purely bound surface plasmon modes in SPP waveguides. Their definition is based on forming benefit-to-cost ratios where the benefit is confinement and the cost is attenuation. Different ways of measuring confinement led to different definitions. The first FoM, $M_1^{1D} = 1/\delta_w\alpha_z$, uses the inverse mode size ($\delta_w$) as its confinement measure, where $\delta_w$ is the distance between the 1/*e* field magnitude points of the main transverse electric field component relative to the global field maximum. The second FoM, $M_2 = (\beta_z - \beta_1)/\alpha_z = (n_{eff} - n_1)/k_{eff}$ measures confinement as the mode's distance from the light line in the dielectric. The third FoM, $M_3 = 1/\lambda_g\alpha_z = \beta_z/2\pi\alpha_z = n_{eff}/2\pi k_{eff}$, uses the inverse guided wavelength $\lambda_g$ as its confinement measure. $M_3$ is proportional to the quality factor ($Q$) when dispersion is negligible.

### *2.2 Definition of the figure of merit $M_1^{2D}$ for 2D waveguides*

The definition of $M_2$, and $M_3$ holds for modes in 2D waveguides, but the definition of $M_1$, which is based on mode size, depends on the dimensionality of the structure as emphasized in [26]. For 1D waveguides, the mode size is the width $\delta_w$, leading to $M_1^{1D}$. For 2D waveguides, the mode size is an area, leading to a new definition for $M_1$, denoted $M_1^{2D}$.

The mode size is taken as the area $A_e$ bounded by the closed 1/*e* field magnitude contour relative to the global field maximum. The 2D spatial distribution in the transverse plane of the main transverse electric field component is used to find this contour and the area $A_e$. The contour and $A_e$ are determined numerically, so highly deformed modes, sometimes supported by SPP waveguides, are easily and unambiguously handled.

Taking the confinement measure as $(\pi/A_e)^{1/2}$, instead of simply $1/A_e$, seems preferable since this measure tends to the inverse mode radius as the mode becomes circular and it leads to a unit-less FoM. This confinement measure also tends to zero as the mode expands or as the waveguide evolves into a 1D structure (as it should since confinement is lost along one of the transverse dimensions). Based on these considerations, the $M_1^{2D}$ FoM is defined as:

$$M_1^{2D} = \sqrt{\frac{\pi}{A_e}}\frac{1}{\alpha_z} \tag{1}$$

## 3. Geometric study of metal stripe waveguides

The waveguides considered are shown in Fig. 1, and consist of (a) the metal stripe ($w < \infty$) and slab ($w = \infty$), (b) and (c) 2 and 3 symmetrically coupled (SC) metal stripes, and (d) the cladded metal stripe. The cladded metal slab ($w = \infty$) was analyzed in [27], and the cladded metal stripe was recently reported in [28] and added to this paper during revisions. The metal stripe on a thin dielectric layer or membrane (not shown) was recently introduced in [29] and bears points of similarity to the cladded metal stripe [28]. The metal slab was analyzed using the transfer matrix method [30]. A commercial software package based on the finite element

#84184 - $15.00 USD Received 15 Jun 2007; revised 3 Sep 2007; accepted 3 Sep 2007; published 10 Sep 2007

method (Femlab) was used to model the 2D structures. This package has been shown to accurately model surface plasmon waveguides [31]. Only the $s_b$ and $ss_b^0$ modes are considered and compared. $\lambda_0$ was set to 1550 nm, Au was used as the stripe metal ($\varepsilon_{r,m} = -\varepsilon_R - j\varepsilon_I = -131.95 - j12.65$ [32]), with the surrounding dielectric being $SiO_2$ ($\varepsilon_{r,1} = n_1^2 = 2.085$ [32]) and, additionally, vacuum ($\varepsilon_0$) in the case of the cladded stripe (Fig. 1(d)).

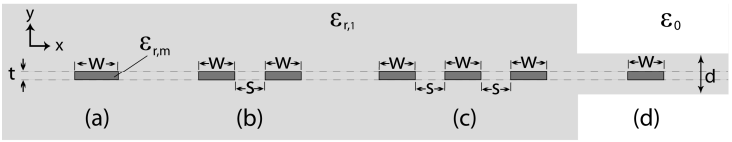


Fig. 1. Cross sectional view of surface plasmon waveguides. (a) Single stripe, (b) pair of SC stripes, (c) three SC stripes, (d) cladded stripe.

The metal stripes (Figs. 1(a)-(c)) are discussed first. Figs. 2(a) and (b) give the effective index ($n_{eff}$) and attenuation ($\alpha_z$, $k_{eff}$) of the $s_b$ and $ss_b^0$ modes as a function of $t$. The usual trends of $n_{eff} \rightarrow n_1$ (vanishing confinement) and $\alpha_z$, $k_{eff} \rightarrow 0$ (vanishing attenuation) as $t \rightarrow 0$ are noted.

Figure 2(c) shows that as $t$ decreases, the mode size increases for all structures considered, as expected. From Fig. 2(d), it is noted that $M_1^{1D}$ and $M_1^{2D}$ increase for all structures as $t$ and/or $w$ decrease, indicating that $\alpha_z$ decreases more rapidly than the modes' expansion. Given a mode size $(A_e/\pi)^{1/2}$, single narrow thick stripes are better than wide thin ones or coupled ones, since they generate less attenuation yielding a larger $M_1^{2D}$. For a specific $t$ narrower stripes produce a larger $M_1^{2D}$ than wider ones.

The modes' distance from the light line, plotted in Fig. 2(e), decreases with $t$ and $w$ as expected since the modes evolve into the TEM wave of the background as the metal vanishes. From Fig. 2(f) it is noted that $M_2$ increases sharply with decreasing $t$, reaching a peak beyond which it tends to 0 as $t \rightarrow 0$. These peaks are located at $t$ = 18 nm for the $w$ = 2 μm stripe, at $t$ = 10 nm for the $w$ = 8 μm stripe, at $t$ = 9.5 nm for the $wswsw$ = 22222 μm SC stripes, and at $t \sim 0$ for the $s_b$ mode in the slab. On the thicker side of the peaks, $k_{eff}$ decreases more rapidly than the confinement ($n_{eff} - n_1$) as $t$ is reduced, but the opposite holds true on the thinner side of the peak. Given a distance from the light line ($n_{eff} - n_1$), single wide thin stripes perform better than narrow thick ones or coupled ones, since they generate less attenuation, yielding a larger $M_2$. For a specific $t$ wider waveguides produce a larger $M_2$ than narrower ones. These trends are opposite to those observed from $M_1^{2D}$.

$\lambda_g$ plotted in Fig. 2(g) increases with decreasing $t$ and $w$. $M_3$, plotted in Fig. 2(h), shows a similar trend to the other FoMs in that $M_3$ increases with decreasing $t$. This implies that $\alpha_z$ decreases more rapidly than $\lambda_g$ increases as $t$ is reduced. Given a $t$ narrower waveguides are better than wider ones leading to a larger $M_3$, as observed for $M_1^{2D}$.

The cladded metal stripe (Fig. 1(d)) [28] is similar to the metal stripe on a thin dielectric membrane [29], in that as the thickness of the dielectric changes, the $ss_b^0$ mode may become more confined and attenuated. Another point of similarity rests with the conditions for $ss_b^0$ confinement, which are that its $n_{eff}$ must be larger than $n_1$ and than the $n_{eff}$ of the $TM_0$ mode in the dielectric slab present to the left and right of the metal stripe. If TM-TE mode conversion is expected, say due to discontinuities, then it should also be larger than the $n_{eff}$ of the $TE_0$ mode of the dielectric slab, but this condition is essentially otherwise irrelevant as was demonstrated experimentally in [29] since the $ss_b^0$ and $TE_0$ modes are substantially orthogonal. In a symmetric slab, the $TM_0$ and $TE_0$ modes are guided for all dielectric thicknesses. Another point of similarity rests with the excitation of the waveguides, in that if the source and $ss_b^0$ mode fields are not well matched then light becomes trapped in the dielectric slab and may interfere with the $ss_b^0$ mode. This may be problematic in structures such as couplers and Mach-Zehnder interferometers.

#84184 - $15.00 USD Received 15 Jun 2007; revised 3 Sep 2007; accepted 3 Sep 2007; published 10 Sep 2007

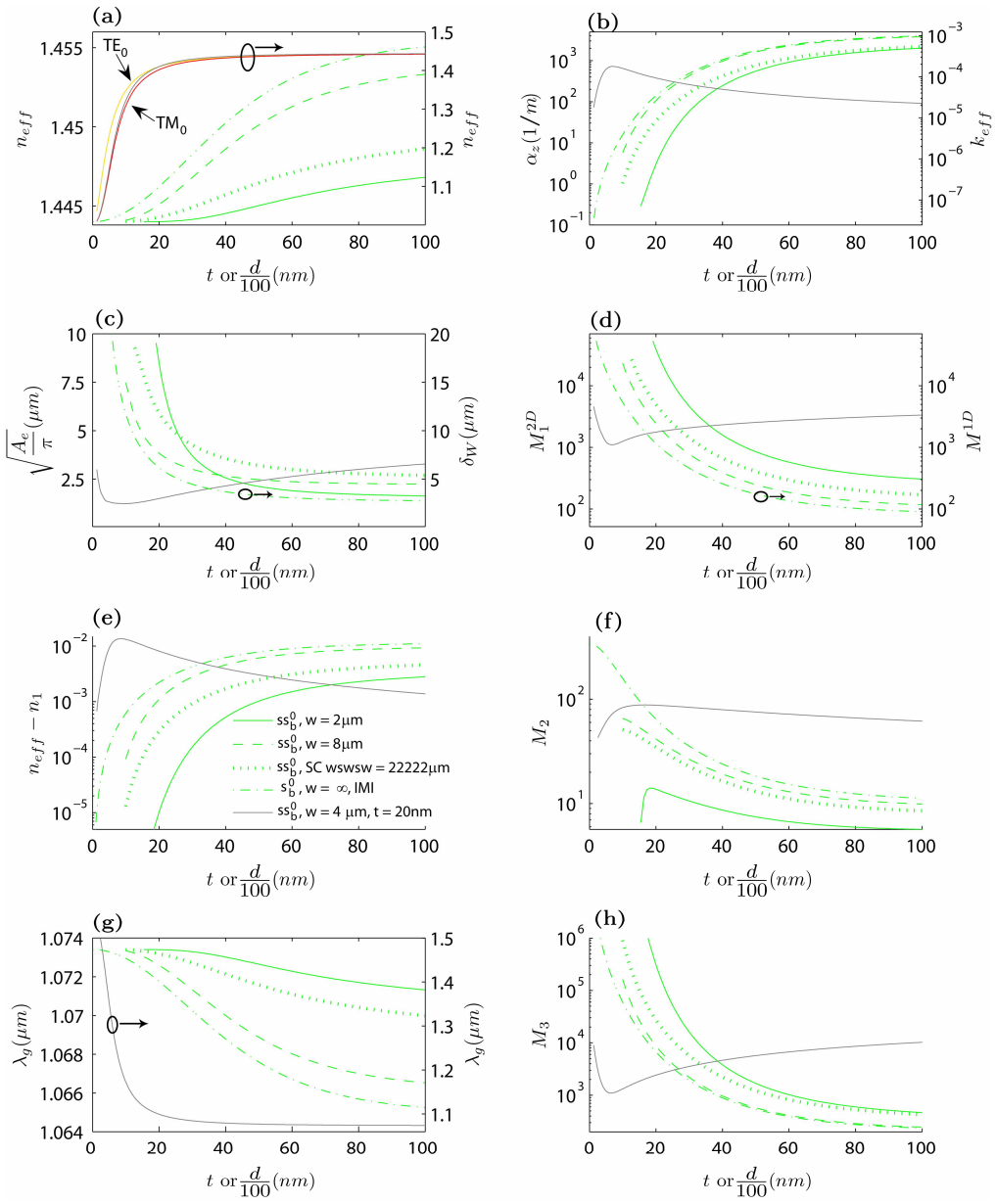


Fig. 2. (a) $n_{eff}$ and (b) $\alpha_z$ and $k_{eff}$ of the $ss_b^0$ and $s_b$ modes. (c) Mode size for the $s_b$ mode in the slab (right axis) and the $ss_b^0$ mode in the stripes (left axis). (d) $M_1^{1D}$ (right axis) and $M_1^{2D}$ (left axis). (e) Distance from the light line and (f) $M_2$. (g) Guided wavelength and (h) $M_3$. The gray curves are for the cladded stripe (Fig. 1(d)).

Figure 2(a) shows $n_{eff}$ of the $ss_b^0$ mode in the cladded metal stripe for $w$ = 4 μm and $t$ = 20 nm, as well as $n_{eff}$ of the $TM_0$ and $TE_0$ modes in the dielectric slab alone, as a function of $d$. From Fig. 2(a) we see that $n_{eff}$ of the $ss_b^0$ mode is always larger than that of the $TM_0$ mode, while it falls below that of the $TE_0$ mode for $d \sim 1.9$ μm. $n_{eff}$ of the $ss_b^0$ mode decreases as $d$ decreases, which is expected since the mode fields extend further into the vacuum. In Fig. 2(b) $\alpha_z$ increases with $d$ until a maximum, from which it drops quickly. The mode size plotted in Fig. 2(c) decreases with decreasing $d$ until a minimum is reached around $d$ = 900 nm. For smaller $d$ the mode extends deeper into the vacuum, explaining the decreasing $\alpha_z$ and $n_{eff}$.

#84184 - $15.00 USD Received 15 Jun 2007; revised 3 Sep 2007; accepted 3 Sep 2007; published 10 Sep 2007

Indeed, the mode tends toward cut-off ($n_{eff} \sim n_1$) in this region. $M_1^{2D}$ plotted in Fig. 2(d) decreases with decreasing $d$, implying that $\alpha_z$ increases more rapidly than the confinement measured as the mode size, until $d \sim 675$ nm beyond which the opposite trend holds. The distance from the $TM_0$ mode is plotted in Fig. 2(e) instead of the distance from the light line, i.e.: $n_{eff}$ of the $TM_0$ mode is used instead of $n_1$ since it is larger. The corresponding $M_2$ plotted in Fig. 2(f) increases with decreasing $d$ up to a peak at $d \sim 1.67$ μm, indicating that the confinement measured as this distance increases more rapidly than $k_{eff}$. Decreasing $d$ decreases $\lambda_g$ as shown in Fig. 2(g). The corresponding $M_3$ plotted in Fig. 2(h) shows a similar trend to $M_1^{2D}$, decreasing with $d$ until $d \sim 650$ nm.

It is noted that $M_1^{2D}$, $M_2$ and $M_3$ of the cladded metal stripe (Fig. 1(d)) are larger than those of the metal stripe (Fig. 1(a), $d = \infty$) over a good range of dimensions, indicating that the former can provide a better trade-off between confinement and attenuation, as noted in [28]. It must be borne in mind, however, that the metal stripe must have a smaller $t$ or $w$ or both as $d$ decreases in order to maintain the same $\alpha_z$ and thus the same range as the $d = \infty$ case. Producing high quality metal stripes can be challenging for $t < 20$ nm [33].

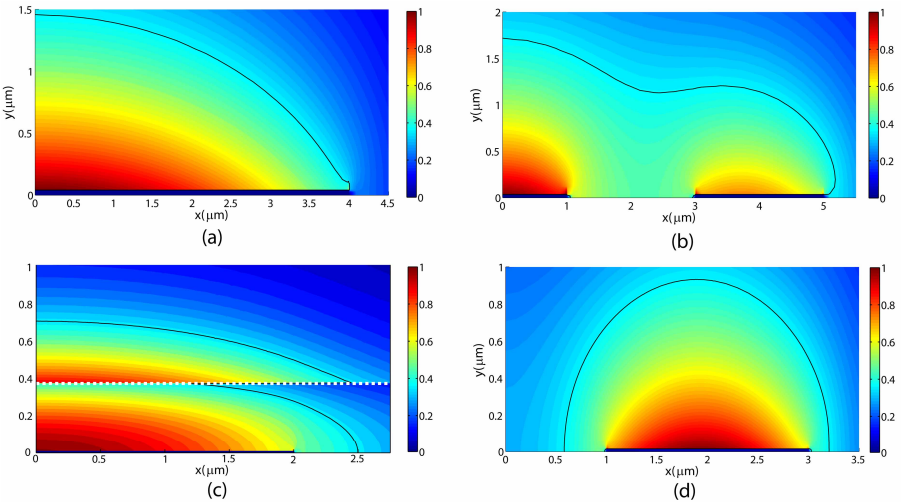


Fig. 3. Spatial distribution of $|E_y|$ associated with the $ss_b^0$ mode in various waveguides. Quarter symmetry is used with the origin, ($x = y = 0$), being the center of the mode. The 1/e field contour is also plotted as the thin black curve. In all cases, the fields are normalized such that $\max(|E_y|) = 1$. (a) Single stripe with $w = 8$ μm and $t = 70$ nm; the associated movie shows a sweep over $t$. (b) Three SC stripes with $wswsws = 22222$ μm and $t = 70$ nm; the associated movie shows a sweep over $t$. (c) Cladded stripe with $w = 4$ μm, $t = 20$ nm and $d = 0.8$ μm; the associated movie shows a sweep over $d$. (d) Pair of SC Au stripes, $wsw = 222$ μm, $t = 30$ nm and $\lambda_0 = 1000$ nm; the associated movie shows a sweep over $\lambda_0$.

Figures 3(a), (b) and (c) give the spatial distribution of $|E_y|$ associated with the $ss_b^0$ mode in a single stripe having $w = 8$ μm and $t = 80$ nm, in three SC stripes having $wswsw = 22222$ μm and $t = 70$ nm and in a cladded stripe having $w = 4$ μm and $t = 20$ nm, respectively. The $1/e$ field contour is plotted as the thin black curve and the $SiO_2$-vaccuum interface is shown as the dashed white line in Fig. 3(c). There is also an inner contour(s) that exists near the surface of the stripe(s), which depends on the penetration of $|E_y|$ into the metal. In the case of Figs. 3(a) and (c), the area $A_e$ is the area within the outer closed contour, not including the area within the inner closed contour since the field enclosed by the latter has a magnitude below the $1/e$ level. The movies associated with Figs. 3(a) and (b) show how the mode evolves with $t$. Both waveguides show the field and $1/e$ contour extending further into the dielectric as $t$ is reduced. This decrease in confinement also causes the mode field to become more circular, more closely matching that of a single mode fiber. This can be seen in the movie in Fig. 3(a) with the mode field almost circular for $t \leq 20$ nm. From the movie in Fig. 3(b), weaker coupling

#84184 - $15.00 USD Received 15 Jun 2007; revised 3 Sep 2007; accepted 3 Sep 2007; published 10 Sep 2007

between the three SC stripes is observed from the shape of the mode field as $t$ and the confinement increase. The movie in Fig. 3(c) shows the mode size decreasing with $d$ until $d \sim$ 900 nm where the 1/$e$ field begins to extend further into the vacuum region.

**4. Wavelength response of metal stripe waveguides**

The FoMs are now used to assess the wavelength response of metal stripe waveguides for three different metals embedded in $SiO_2$: Ag, Au and Al. The optical properties of these materials were taken from the experimentally determined data compiled in Palik [32]. A cubic spline was used to interpolate the permittivity at the desired wavelengths. The waveguides used in the analysis were chosen based on their similar proximity to the light line at $\lambda_0 = 1550$ nm (all have $n_{eff} - n_1 \sim 5\times10^{-4}$, Fig. 2(e)): A single stripe with $w = 2$ μm, $t = 40$ nm, a single stripe with $w = 4$ μm, $t = 20$ nm, and a pair of SC stripes with $wsw = 222$ μm, $t = 30$ nm.

Figure 4(a) shows $n_{eff}$ versus $\lambda_0$ of the $ss_b^0$ mode, along with the light line in $SiO_2$; Fig. 4(b) shows the corresponding $\alpha_z$. An interesting feature arose in the case of Au: $n_{eff}$ of the single interface SPP crosses the light line at $\lambda_0 = 473$ nm (slightly beyond the energy asymptote), while $n_{eff}$ of the slab and of the stripes do not cross the light line at this wavelength. The modes appear to remain bound for $\lambda_0 \geq 250$ nm. This trend does not show up in the case of Ag. The modes supported by the Al waveguides did not reach their energy asymptote for the range of wavelengths used, which makes it unclear as to whether Al would show this feature. Fig. 4(b) shows that lower loss can be achieved when operating deeper into the infrared for all the waveguides and metals analyzed. For all metals, as the wavelength decreases, the $ss_b^0$ mode becomes more localized to the center of the stripe along the metal/dielectric interfaces and the effects of the corners and the dielectric regions on either side diminish.

Figure 4(c) shows that the mode size increases when operating further into infrared. At short wavelengths the curves exhibit features and small peaks which are explained by inspecting the mode fields, revealing that they increase in strength near the corners at specific wavelengths. This behavior also perturbs the 1/$e$ contour associated with the modes.

Figure 4(d) shows that $M_1^{2D}$ increases with increasing wavelength, whereas $M_1^{1D}$ remained flat in the Drude region as observed from Fig. 3 of [26]. The modes supported by the Ag waveguides experience a small drop in $M_1^{2D}$ near $\lambda_0 = 1630$ nm while the Al waveguides show a drop for $\lambda_0$ between 700 and 900 nm. Looking at Fig. 4(b), an increase $\alpha_z$ is observed in these regions, which is not matched by an equivalent increase in confinement, causing the dip in $M_1^{2D}$. In the wavelength range around 1630 nm, where the Ag structures show a decrease in $M_1^{2D}$, Au out-performs. Al is a good choice for $\lambda_0 \leq 400$ nm.

From Fig. 4(e) it is noted that the distance from the light line decreases sharply at long wavelengths. Interestingly, $M_2$ plotted in Fig. 4(f), exhibits maxima for Au and Ag. The Ag structures exhibit a peak with its location depending slightly on the geometry: the $w = 4$ μm $t = 20$ nm, $wsw = 222$ μm $t = 30$ nm, and $w = 2$ μm $t = 40$ nm structures have peaks at $\lambda_0 = 845$, 835 and 825 nm, respectively. The corresponding Au structures also exhibit peaks in $M_2$ near these wavelengths, but they are broader and lower than those of the Ag structures. Ag outperforms Au over a broad wavelength range but beyond 1630 nm Au seems better. $M_2$ decreases sharply on the long wavelength side of the peak, in keeping with the rapid loss of confinement noted earlier from Fig. 4(e). Based on $M_2$, it is preferable to operate Au and Ag waveguides near the short wavelength limit of the Drude region, as was already observed for Ag in [26]. The modes supported by the Al waveguides show a decrease in $M_2$ for $\lambda_0$ in the range of 400 to 900 nm. The Al waveguides again perform better than the Au and Ag ones for $\lambda_0 \leq 400$ nm, while being considerably outperformed throughout the rest of the spectrum.

Figure 4(f) shows the quality factor $Q$. (In the calculation of $Q$, the derivative in Eq. (18) of [26] was estimated using finite difference approximants.) $M_3$ is shown in Fig. 4(h). When the modes experience minimal dispersion, as they do in the Drude region, then $Q \sim \pi M_3$, as is observed by comparing these Figs. In the short wavelength region the modes experience a large change in their $n_{eff}$ as they approach the energy asymptote, causing a greater difference between $Q$ and $M_3$. Both sets of curves show a similar trend to $M_1^{2D}$, where the Au and Ag

#84184 - $15.00 USD Received 15 Jun 2007; revised 3 Sep 2007; accepted 3 Sep 2007; published 10 Sep 2007

structures outperform the Al ones for $\lambda_0 \geq 400$ nm. Silver outperforms Au for $\lambda_0 \geq 400$ nm until about 1630 nm, where Au appears to be better.

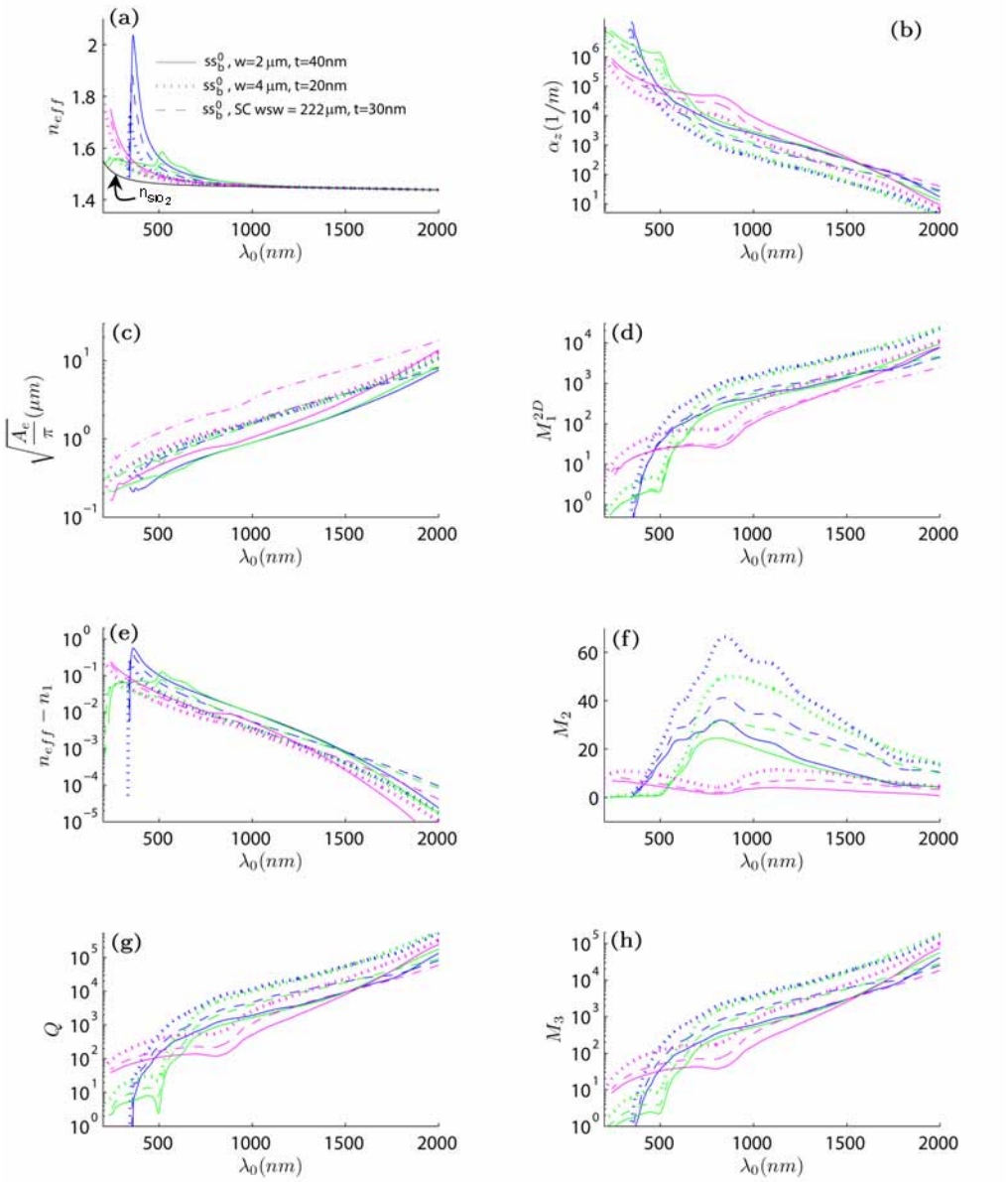


Fig. 4. (a) $n_{eff}$ and (b) $\alpha_z$ versus $\lambda_0$. (c) Mode size and (d) $M_1^{2D}$. (e) Distance from the light line and (f) $M_2$. (g) Quality factor $Q$ and (h) $M_3$. (green: Au, blue: Ag, magenta: Al)

Figure 3(d) gives the spatial distribution of $|E_y|$ associated with the $ss_b^0$ mode in two SC Au stripes having $wsw$ = 222 μm and $t$ = 30 nm. The associated movie shows how the mode evolves with decreasing $\lambda_0$. As the mode approaches its energy asymptote, it becomes more confined and localized to the center of the stripe along the metal/dielectric interfaces. At short $\lambda_0$, the coupling between the stripes weakens, eventually disappearing altogether.

#84184 - $15.00 USD Received 15 Jun 2007; revised 3 Sep 2007; accepted 3 Sep 2007; published 10 Sep 2007

## 5. Summary and concluding remarks

The FoM $M_1^{2D}$ was defined for 2D waveguides as the ratio of $(\pi/A_e)^{1/2}$ to $\alpha_z$.. Using this FoM, along with those proposed in [26], a quantitative comparison of metal stripe waveguides supporting the $ss_b^0$ mode was performed as a function of stripe geometry, stripe metal and $\lambda_0$, assuming $SiO_2$ as the background dielectric. Depending on how confinement is measured, and thus on which FoM is used, then different conclusions on waveguide quality are reached.

Various geometries were considered for Au stripes at $\lambda_0 = 1550$ nm. The analysis showed that, for a given $t$, narrower single stripes maximize both $M_1^{2D}$ and $M_3$, while $M_2$ is maximized by wider single stripes. Also, given a mode area, single narrow thick stripes are better than wide thin ones or coupled ones, according to $M_1^{2D}$. $M_2$ yields an opposite result, where given a distance from the light line, single wide thin stripes are better than narrow thick ones or coupled ones.

The cladded metal stripe was also considered, yielding larger FoMs over a good range of dimensions and hence a better confinement-attenuation trade-off than the stripe. It was noted though that in order to match the range of the stripe, the metal thickness and/or width needed to be decreased, which could challenge fabrication.

The wavelength response of various structures was computed for Au, Ag and Al as the stripe. Operating at longer wavelengths maximizes $M_1^{2D}$ and $M_3$, in contrast to $M_1^{1D}$ which remained flat [26]. $M_2$ exhibits well-defined maxima for Au and Ag at $\lambda_0 \sim 850$ nm (near the short wavelength limit of the Drude region), varying slightly depending on the geometry. Based on all of the FoMs, Al provides the best performance for $\lambda_0 \leq 400$, with Au possibly being better for $\lambda_0 > 1630$ nm and Ag performing better throughout the rest of the spectrum. These conclusions, which depend on the measured optical parameters of the metals collected in [32], should also hold for other 2D SPP waveguides (e.g.: [23-25]).

#84184 - $15.00 USD Received 15 Jun 2007; revised 3 Sep 2007; accepted 3 Sep 2007; published 10 Sep 2007